Process Parameter Optimization and Crack Density Prediction in Laser Cladding Using a BP Neural Network Model

Jixia Li, Weigang Zeng*, Rongfan Zhao, Youzhong Jiang, Jun Guo and Wei Gao College of Mechanical Engineering, Karamay Vocational and Technical College, Karamay 834000, China

E-mail: kzy2023034@163.com *Corresponding author

Keywords: laser cladding; crack sensitivity; orthogonal test; neural network; process optimization

Received: April 13, 2025

To address the crack defects arising from the complex nonlinear mapping relationship between key laser cladding process parameters and coating preparation, this study conducted a theoretical analysis and experimental verification by employing a BP neural network to predict crack density based on orthogonal experimental data. Initially, a three-factor four-level orthogonal experiment was performed to obtain fundamental sample data for the neural network, followed by dataset expansion using kernel density estimation (KDE). The dataset was then preprocessed through min-max normalization, ultimately establishing a three-layer predictive neural network model that correlates laser cladding layer process parameters (powder feeding rate, overlap rate, and scanning speed) with crack susceptibility. The results demonstrate that the BP neural network model achieves crack density predictions with relative errors fluctuating within $\pm 5\%$, while maintaining an average error of 0.85% and a mean square error of 1.11%, indicating high prediction accuracy and stable performance. Furthermore, a comparative analysis of various regression methods, including KNN, Ridge, and Random Forest, was conducted in terms of R², RMSE, and MAE metrics, revealing that the BPNN exhibits superior comprehensive performance. These findings validate the feasibility of applying BP neural networks for crack density prediction through process parameters in laser cladding applications, which holds significant importance for fabricating crack-free nickel-based cladding layers.

Povzetek: Študija z ortogonalnimi eksperimenti in razširitvijo podatkov (KDE) vzpostavi BP-nevronski model, ki iz procesnih parametrov (dovod prahu, prekrivanje, hitrost skeniranja) napoveduje gostoto razpok pri laserskem navarjanju Ni60 ter podpira optimizacijo postopka glede na razpoke odporne obloge.

1 Introduction

With the continuous development of laser cladding technology, it has shown many advantages in the manufacturing of large and complex metal workpieces and metal surface strengthening processes [1]. Laser cladding is an advanced manufacturing method that uses highenergy laser beams to rapidly melt and solidify powder and substrate. However, due to the complex process of integrating multiple physical fields in laser cladding, the interaction between process parameters such as powder feeding rate, laser power, laser scanning speed, etc. will affect the quality of the deposited metal layer [2]. The coating is prone to serious cladding defects such as cracks [3], especially when cladding materials with higher hardness, which greatly limits the development, and application of laser cladding technology [4, 5]. Using traditional process experiments to control cracks is time-consuming, labor-intensive, and wasteful of resources, and the effect is average. How to comprehensively and intelligently control the factors that

affect the cladding process is a hot research direction in this field [6, 7].

In this study, we investigated the challenge of crack formation in high-hardness nickel-based coatings by examining the key influencing factors of laser cladding crack generation and analyzing the feasibility of achieving crack density prediction errors below 10% using a threelayer BP neural network based on orthogonally designed input parameters. Previous research has demonstrated the application of BPNN in establishing mapping relationships between laser cladding parameters and coating characteristics, as summarized in Table 1. Ni and Liu from Central South University in Hunan Province optimized the melting process using neural networks and particle swarm optimization methods [8]; Huang et al. from Huazhong University of Science and Technology used neural networks to predict the characteristics and properties of aluminum alloy cladding layers [9]; Jiang et al. from the Shenyang Research Institute of the Chinese Academy of Sciences used neural networks to study the prediction of cladding height [10]; Yang et al. from Northwestern Polytechnical University used neural networks to predict

the morphology and quality of laser formed parts [11]; Lei et al. from Wuhan University of Technology studied the prediction of characteristic parameters of broadband laser cladding pool using neural networks [12]; Liu et al. from the School of Mechanical Engineering, Hubei University of Technology studied the prediction of the morphology of

nickel based alloy overlay layer using GA-BP neural network [13]. However, it is not difficult to find that most scholars still mainly use BPNN to predict the height, width, morphology and other characteristics of the cladding layer, and lack comprehensive multi factor intelligent crack prediction research for higher hardness cladding layers.

Table 1: Comparison of model performance characteristics

| Reference number | Model Name | Prediction Target | Model Mapping Relationship | Quantitative Result |
|---------------------|------------|--|---|---|
| 7 | BPNN+PSO | Characteristics of the cladding layer - height and width | The relationship between cladding bead characteristics (width, height) and cladding process parameters | Relative errors less than 4.5% |
| 8 | ANN | Prediction of characteristics and properties of aluminum alloy cladding layers | The relationship between laser cladding process parameters and the characteristics/properties of cladding layers | The maximum error value is 12.5% |
| 9 | BPNN | Prediction of clad height | The relationship between laser process parameters and clad height | Mean squared error of 0.0091 |
| 10 | BPNN | Prediction of surface quality in formed components | The relationship between scanning speed and infill angle during laser additive manufacturing and the surface quality evaluation parameters of fabricated components | MSE < 0.01 |
| 11 | GA-BP | Prediction of coating morphology | The mapping relationship between laser processing parameters and the macroscopic morphology of cladding layers | Average relative error of 3.951% |
| 12 | BPNN | Prediction of melt pool characteristics in wide- band laser cladding | The relationship between laser cladding process parameters (laser power, powder thickness, scanning speed) and melt pool characteristic parameters | Errors less than 2% and correlation coefficient R approaching 1 |

Therefore, from the perspective of crack sensitivity analysis, in order to better meet the quality requirements of the cladding layer, the mechanism of crack formation was theoretically analyzed, and the cladding parameters were determined to be important factors leading to crack formation. Through the Analytic Hierarchy Process (AHP),

it was clarified that process parameters such as powder feeding rate, overlap rate, and scanning speed had the greatest impact on crack sensitivity. Then, by designing a 3-factor 4-level orthogonal experiment, sample data of crack density was collected. Based on the data provided by the orthogonal experiment, the data was expanded through

interpolation, and a neural network model was constructed with the processed sample data as a reference, achieving a nonlinear mapping relationship between various process parameters and crack density.

The contribution of this article is to propose a neural network prediction model based on small sample data on the basis of a small number of experiments. It can accurately predict crack density through process parameters such as powder feeding rate, overlap rate, and scanning rate. This can reduce the amount of process experiments, save materials, and analyze the impact of uncertain nonlinear factors on cracks in laser cladding layers with high hardness. At the same time, it provides a feasible new approach to reduce the number of offline experiments and prepare crack free coatings.

2 Experimental materials and methods

Through the study of coating cracks, 45# steel was selected as the substrate, with a substrate size of 110 mm×60 mm×6 mm and a quantity of 16 pieces. In order to minimize the effect of external factors on the cladding layer, the steel plate was polished and polished before using the 45# steel substrate. Then, the surface of the steel plate to be clad was cleaned with anhydrous ethanol to ensure that the substrate surface was flat and free of rust, oil, and other impurities. Ni60 powder is selected as the laser cladding powder, with a powder size of 140-325 mesh. Due to the fine powder, it is prone to moisture absorption and agglomeration in the air, which affects the experimental results. Therefore, it is necessary to dry and remove the powder before use. The element content in the 45-steel matrix is shown in Table 2, and the element content in the Ni60 self-melting laser cladding powder is shown in Table 3.

2.1 Experimental materials

Table 2: Contents of elements in 45# steel (w%)

| Element | Cr | Si | C | Mn | Ni | Cu | Fe |
|--------------------------|-------|-----------|-----------|-----------|-------|--------|---------|
| 45 # steel quality score | ≤0.25 | 0.17-0.40 | 0.42-0.50 | 0.50-0.80 | ≤0.25 | ≤ 0.30 | Balance |

Table 3: Content of elements in Ni60 self-melting powder (w%)

| Element | C | Cr | В | Si | Fe | Ni |
|--------------------|---------|-----------|---------|---------|-------|--------|
| Ni60 quality score | 0.7-1.0 | 14.0-17.0 | 3.0-4.5 | 3.5-5.5 | ≤15.0 | Margin |

2.2 Experimental equipment and methods

The German KUKA machine KR30HA was used in the experiment; Experimental research was conducted on the Xinsong XSL-PF-01B-2 synchronous side powder feeder; The protective gas used in the experiment is argon gas; The cooling system uses a dual temperature chiller unit, model PH-LW296-TH2P; The fusion equipment is undergoing testing as shown in Figure 1.



Figure 1: Experimental equipment

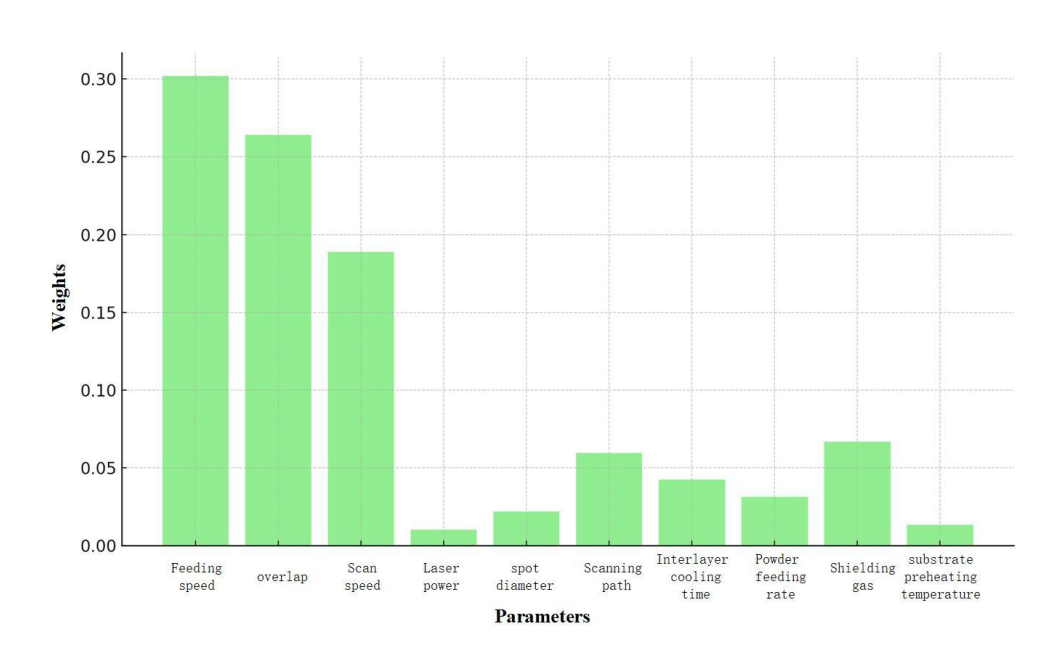


Figure 2: Results of the analytic hierarchy process (AHP) analysis

In general, process parameters such as spot diameter, scanning path, interlayer cooling time, powder feeding rate, protective gas, substrate preheating temperature, laser power, powder feeding speed, overlap rate, and scanning speed all affect the performance and morphology of coatings. The weight of process parameters such as spot diameter and scanning path to crack density was calculated using the Analytic Hierarchy Process (AHP), and the results are shown in Figure 2. Among them, the three process parameter variables of powder feeding speed,

overlap rate, and scanning speed have the highest weight proportion to the results.

Meanwhile, the correlation analysis method was used to compare the correlation sensitivity between different parameters. As shown in Figure 3, the three process parameters of powder feeding speed, overlap rate, and scanning speed have the highest correlation with each other. In summary, the three parameters that have the greatest impact on coating performance and morphology and have a high correlation with each other, namely

powder feeding speed, overlap rate, and scanning rate, were selected as variables for the cladding experiment.

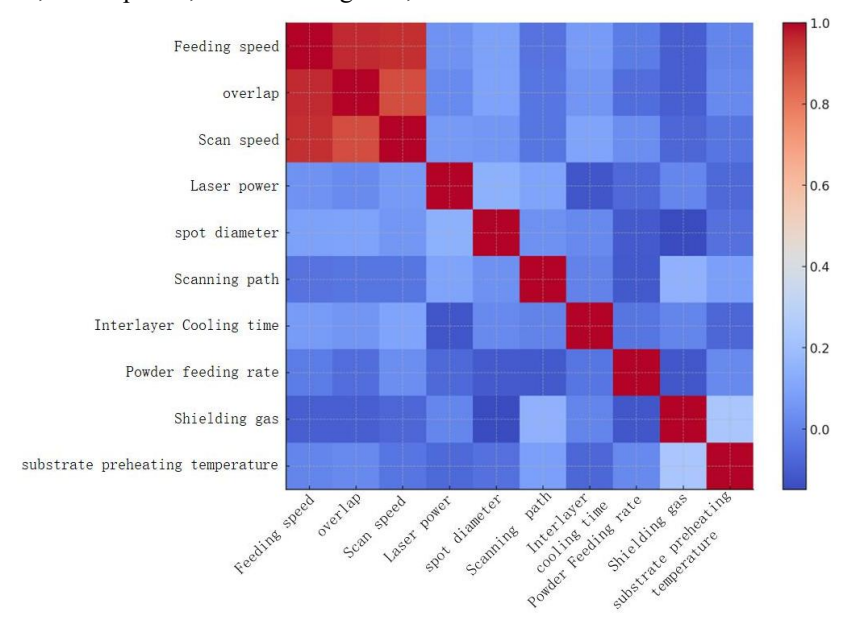


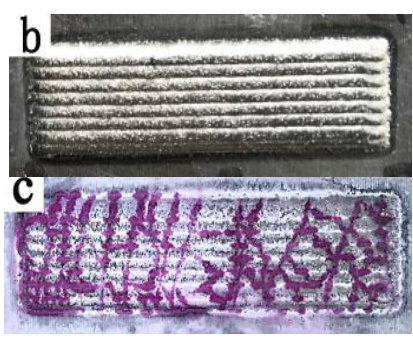
Figure 3: Results of correlation analysis

Due to the hardness of Ni60 powder, in the fusion process, only the powder feeding amount is changed. If other parameters remain unchanged, the total output energy of the laser remains unchanged. If the powder feeding amount is too large, most of the heat source is absorbed by the powder, and the heat reaching the substrate is relatively small. The temperature difference between the substrate and the fusion layer is large, and it rapidly cools at room temperature, resulting in an increase in crack generation; The powder feeding amount is too small, and the thickness of the cladding layer is thin. Due to the high energy of the laser delivered to the substrate, sintering may occur, and the thin cladding layer cannot achieve the purpose of laser repair. If there are multiple overlapping layers and other process parameters remain constant, excessive overlapping rate will result in over overlapping phenomenon. As the number of overlapping times increases, the cladding layer will gradually become thicker, and the surface of the cladding layer will tilt at a certain angle. The temperature gradient between the substrate and the cladding layer will gradually increase. If the overlapping rate is too low, it will lead to excessive surface ripples. Controlling the scanning speed of a single variable, under certain conditions, the crack sensitivity increases with the increase of scanning speed. Due to the fast-scanning speed, there is less heat input on the substrate, making it difficult for the substrate to form a fully melted

melt pool with the powder, resulting in an increase in crack sensitivity [14].

Orthogonal experiments have two distinct characteristics, one is average dispersion, and the other is homogeneity and comparability. The so-called average dispersion refers to the equal occurrence of factor levels in each column; The so-called neat comparability refers to any pair of equivalent numbers in any two columns as a logarithm, where all possible pairs have the same number of repetitions. Based on the three variables of powder feeding speed, overlap rate, and scanning rate, a three factor four level orthogonal experiment L_{16} (4³) was designed. The range of process parameters is shown in Table 4. The fusion experiment was conducted using a fusion robot, and each sample was subjected to 8 overlapping fusion layers. Then, non-destructive crack detection was performed using dye penetrant testing agent to measure and calculate the total length of cracks and the area of the fusion layer of each sample. The crack density was calculated by dividing the two, and to eliminate accidental errors and ensure data accuracy, the final crack density was determined by taking the average of multiple measurements. The experimental process of feeding 20 (g/min) powder, overlapping 50%, and scanning rate 10 (mm/s) is shown in Figure 4.





a-matrix; b-Laser cladding results; c-Nondestructive testing results

Figure 4: Test process

Table 4: Orthogonal experimental parameters

| | Factor | | | |
|-------|---------------------------------|---------------|------------------------|--|
| Level | powder feeding amount / (g/min) | lap rate / (% | scanning rate / (mm/s) | |
| 1 | 16 | 45 | 4 | |
| 2 | 18 | 50 | 6 | |
| 3 | 20 | 55 | 8 | |
| 4 | 22 | 60 | 10 | |

3 Establishment of neural network model and evaluation of simulation performance

The results of the orthogonal experiments for laser cladding parameters are presented in Table 5. These representative experimental datasets will serve as training and testing samples for the neural network to predict crack density.

3.1 Dataset construction

Table 5: Results of the laser cladding orthogonal test cladding

| Test number | Powder delivery quantity/ (g/min) | overlapping ratio/ | scan rate/ (mm/s) | crack density/ (mm/mm²) |
|----------------|--------------------------------------|---------------------------------------|-------------------|-------------------------|
| number | 1 1 1 | · · · · · · · · · · · · · · · · · · · | 4 | 0.201472 |
| 1 | 16 | 45 | 4 | 0.201472 |
| 2 | 16 | 50 | 6 | 0.312450 |
| 3 | 16 | 55 | 8 | 0.331451 |
| 4 | 16 | 60 | 10 | 0.340142 |
| 5 | 18 | 45 | 6 | 0.234483 |
| 6 | 18 | 50 | 4 | 0.321578 |
| 7 | 18 | 55 | 10 | 0.369252 |
| 8 | 18 | 60 | 8 | 0.426565 |
| 9 | 20 | 45 | 8 | 0.275027 |
| 10 | 20 | 50 | 10 | 0.349855 |
| 11 | 20 | 55 | 4 | 0.352161 |
| 12 | 20 | 60 | 6 | 0.450340 |
| 13 | 22 | 45 | 10 | 0.290522 |

| 14 | 22 | 50 | 8 | 0.334810 |
|----|----|----|---|----------|
| 15 | 22 | 55 | 6 | 0.371483 |
| 16 | 22 | 60 | 4 | 0.478756 |

However, due to the small amount of data obtained from orthogonal experiments, it may affect the learning results of the BP neural network and lead to underfitting. Therefore, based on single crack density values and historical experience values, kernel density estimation (KDE) is used to approximate uniform interpolation, thereby expanding the dataset.

Kernel Density Estimation (KDE) is a non parametric probability density estimation method that can fit distributions based on the characteristics and properties of the data itself, without making any distribution assumptions. For a sample set $\{x_1, x_2, \dots, x_n\}$ consisting of n observations of a continuous random variable X, the KED method estimates the probability density function (PDF) of the random variable X using equation (1), denoted as p(x).

$$\hat{p}(x) = \frac{1}{nh} \sum_{i=1}^{n} K(\frac{x - x_i}{h})$$
 (1)

where $\hat{p}(x)$ represents the estimated PDF, h denotes the bandwidth parameter of KDE, and K(u) is the kernel function. Given n observations of a random variable X, if k values fall within the interval [a, b], then p(x) can be expressed as equation (2):

$$\hat{p}(x) = \frac{k}{n(b-a)} \tag{2}$$

By using a fixed interval [a, b] and changing the size of k to estimate the PDF, the number of observations k among the n observations of the random variable X that fall within the interval [a, b] can be expressed as equation (3):

$$k = \sum_{i=1}^{n} K(\frac{x - x_i}{h}) \tag{3}$$

Taking sample #1 as an example, its measurement results are presented in Table 6.

Table 6: Statistical summary of measurement results for test sample #1

| Cladding bead | 1 bead | 2 bead | 3 bead | 4 bead | |
|---------------------------------------|-----------|----------|----------|----------|----------|
| Crack density / (mm/mm ²) | 0.201683 | 0.104472 | 0.233796 | 0.211206 | Average |
| Cladding bead | 5 bead | 6 bead | 7 bead | 8 bead | 0.201472 |
| Crack density / (mm/mm²) | 0.1617654 | 0.325267 | 0.201031 | 0.172556 | |

The crack densities of eight individual cladding beads were treated as a sample set $\{0.104472, 0.1617654, 0.172556, 0.201031, 0.201683, 0.211206, 0.233796, 0.325267\}$. Using KDE with the Gaussian kernel function, we estimated the probability density function p(x) over the fixed interval defined by the minimum and maximum

values [0.104472, 0.325267]. Uniform interpolation was then performed based on the derived PDF, with results presented in Table 7. The results from each orthogonal experiment can be expanded to 32 data values. Through this expansion process, the 16 sets of orthogonal experimental results yield a total of 512 data samples.

Table 7: Interpolation results of measurement data for test sample #1

| Crack density | Crack density | Crack density | Crack density |
|---------------|---------------|---------------|---------------|
| 0.104472 | 0.172556 | 0.201683 | 0.22476 |
| 0.11879535 | 0.179675 | 0.203588 | 0.229278 |
| 0.1331187 | 0.186794 | 0.205492 | 0.233796 |
| 0.14744205 | 0.193912 | 0.207397 | 0.25209 |

| 0.1617654 | 0.201031 | 0.209301 | 0.270384 |
|------------|----------|----------|----------|
| 0.16446305 | 0.201194 | 0.211206 | 0.288679 |
| 0.1671607 | 0.201357 | 0.215724 | 0.306973 |
| 0.16985835 | 0.20152 | 0.220242 | 0.325267 |

3.2 Establishment of neural network model

BP neural network has strong nonlinear mapping ability, fault tolerance, self-learning and adaptive ability, and has been widely used in engineering prediction. For the analysis of process data, an orthogonal experimental scheme was used to melt the Ni60 cladding layer as a sample for the BP neural network. The experimental results were compared with the predicted values of the neural network for performance evaluation. The neural network algorithm flow is shown in Figure 5.

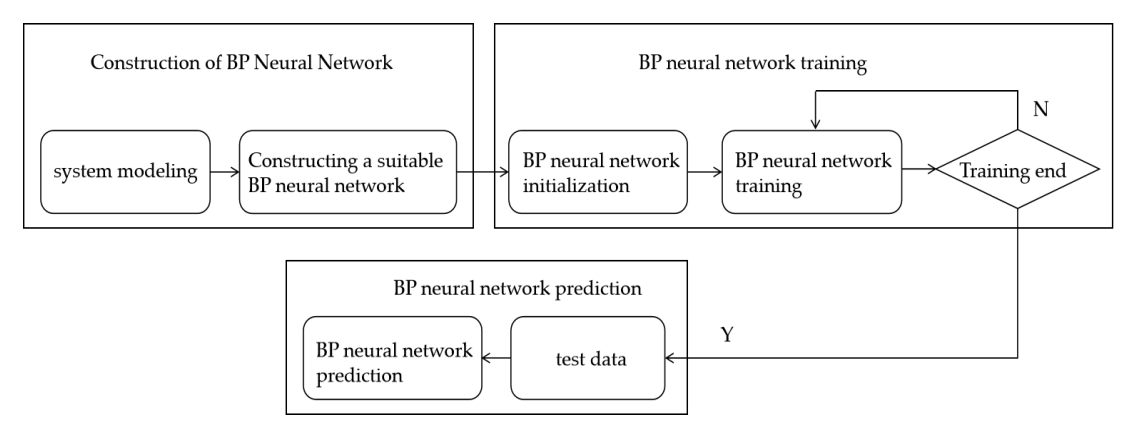


Figure 5: Algorithm flow

A three-layer predictive neural network structure model was established between the process parameters of laser cladding layer and crack sensitivity, as shown in Figure 6. The input layer has three neurons, namely powder feeding rate, overlap rate, and scanning speed, while the output layer only has one neuron, which is crack density. The number of neurons in the hidden layer can be calculated by empirical formula (4).

$$m = \sqrt{A + B} + C \tag{4}$$

In the formulation, A denotes the number of output neurons, B represents the number of input neurons, and C is an empirical constant.

The optimal number of hidden neurons was

determined as 9 (search range: $\{4, 9, 16, 32\}$) through a combined grid search and Bayesian optimization approach, calculated based on input neuron count B and empirical constant Co[1,10], achieving minimal error on the validation set. The network architecture employs ReLU activation for the input layer to ensure computational efficiency, Swish activation in hidden layers to better model nonlinear relationships among process parameters, and linear activation for the output layer to meet regression requirements. To prevent overfitting, the model incorporates L_2 regularization ($\lambda = 0.01$) and a Dropout strategy (rate = 0.3). For the small-scale process data characteristics, the Adam optimizer (learning rate = 0.001, $\beta_1 = 0.9$, $\beta_2 = 0.999$) was selected to ensure training stability and convergence efficiency.

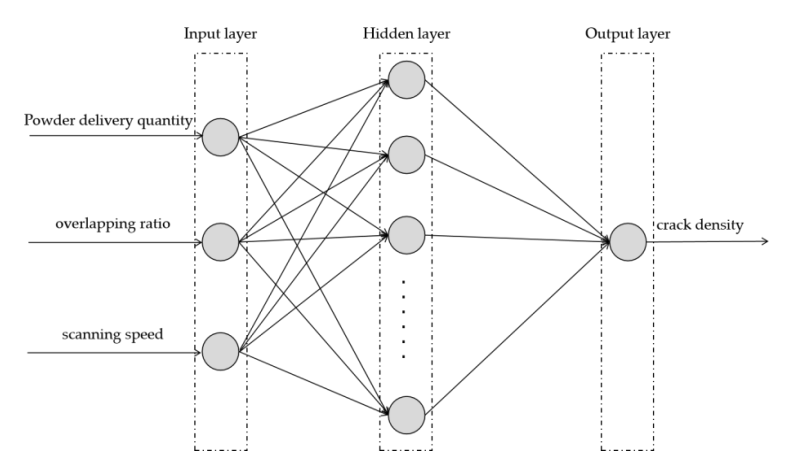


Figure 6: Prediction neural network structure model

3.3 Training and simulation of neural network models

Selecting a certain range of powder feeding amount, overlap rate, and scanning speed as input values during the cladding process to use BP neural network to predict the density of cracks in the cladding layer can effectively control the amount of crack generation. Randomly divide the expanded dataset into a training set and a testing set according to an 8:2 ratio.

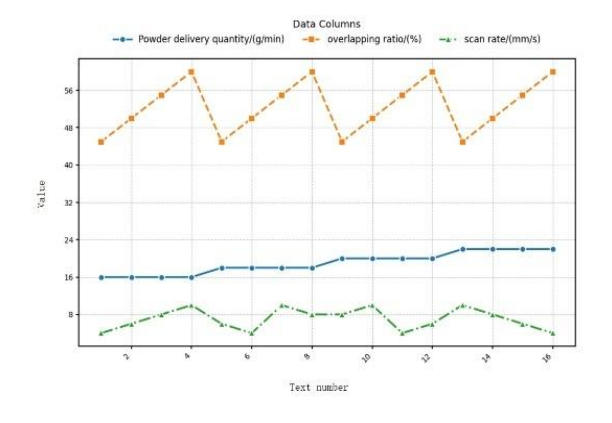
Due to the inconsistent units between various factors and output quantities in orthogonal experiments, it may lead to accuracy errors. Some neural networks have large data volumes, slow convergence, and long training times. In addition, the range of the activation function in their output layer is limited. Therefore, it is necessary to map

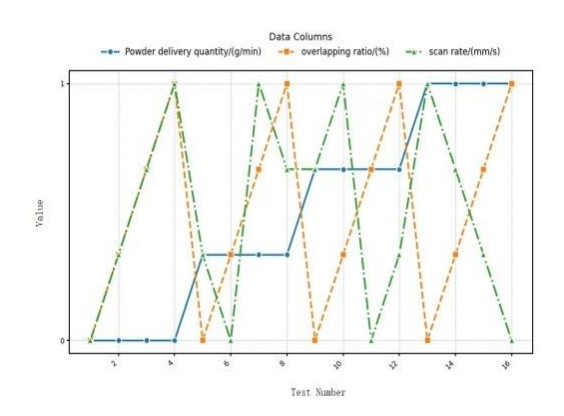
the training target data to the range of the activation function, which requires data normalization. Substitute the three changing parameters and output training values into formula (5), and use the Min Max normalization method to convert the input training value test value and output training value into the range of [0,1].

$$y = \frac{x - x_{\min}}{x_{\max} - x_{\min}} \tag{5}$$

Where, y represents the processed quantity, x is a single sample, \mathbf{x}_{\max} , \mathbf{x}_{\min} and represents the maximum and minimum samples.

As shown in Figure 7, the comparative variation of process parameters before and after normalization is illustrated, with aggregated statistics summarized in Table 8.





a) Process parameters before normalization

b) Normalized process parameters

Figure 7: Process parameters before and after normalization

Table 8: Mean values and standard deviations of normalized process parameters

| Average | | Average | | deviation |
|--------------------|---------------|---------------------|---------------|---------------------|
| Process parameters | Before | After normalization | Before | After normalization |
| | normalization | | normalization | |
| Powder feeding | 19 | 0.5 | 2.309401077 | 0.384900256 |

| amount | | | | |
|---------------|------|-----|-------------|-------------|
| Lap rate | 52.5 | 0.5 | 5.773502692 | 0.384900256 |
| Scanning rate | 7 | 0.5 | 2.309401077 | 0.384900256 |

The model parameters were configured with 1000 maximum iterations and a training target of 1×10^{-6} at a learning rate of 0.01. In practice, the training error dropped below 10^{-6} and stabilized within 150 iterations,

meeting the specified accuracy requirements. The convergence process of the iterative training loss is demonstrated in Figure 8.

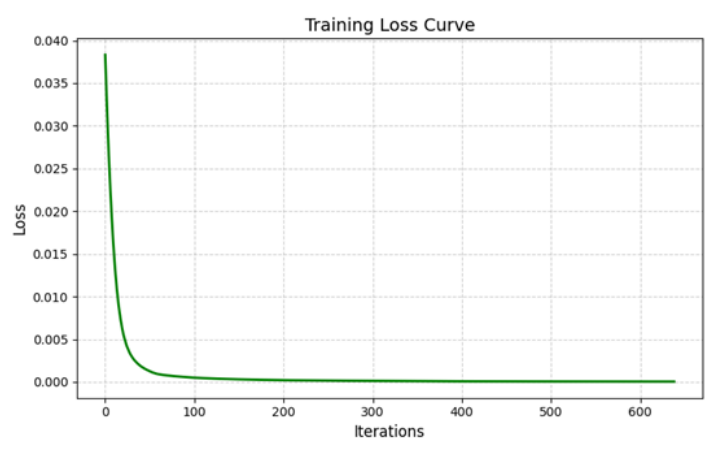


Figure 8: Training loss convergence process

3.4 Performance evaluation of the neural network model

The predictive model's accuracy was comprehensively evaluated using Equations (6)-(9) to calculate four key metrics: relative error (E), mean absolute error (MAE), root mean square error (RMSE), and coefficient of determination (R^2) . This multi-metric assessment framework provides rigorous validation of the model's reliability in predicting crack density.

$$E_{i} = \frac{|y_{i} - \hat{y}_{i}|}{y_{i}} \times 100\%$$
 (6)

$$MAE = \frac{1}{n} \sum_{i=1}^{n} |y_i - \hat{y}_i| \in [0, +\infty)$$
 (7)

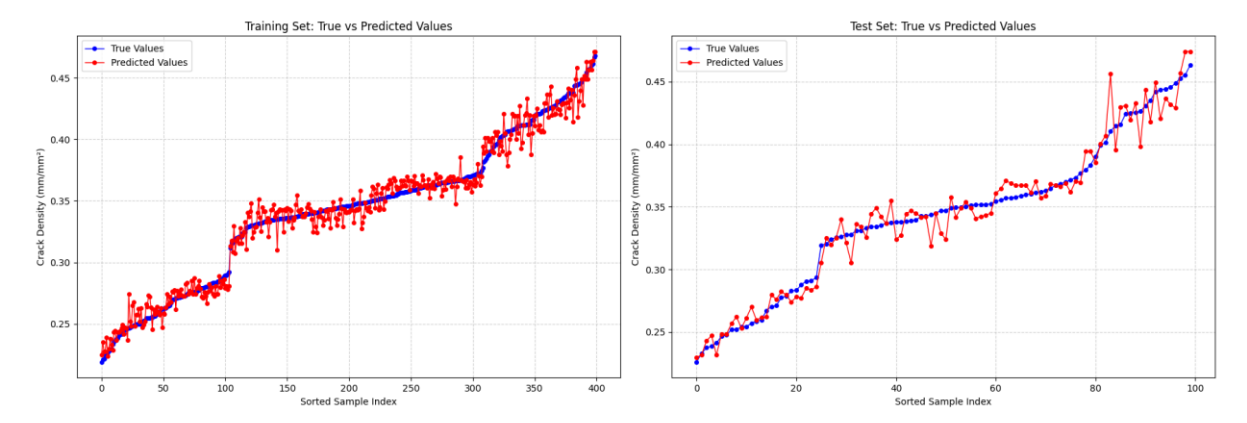
$$RMSE = \sqrt{\frac{1}{n} \sum_{i=1}^{n} (y_i - \hat{y_i})^2}$$
 (8)

$$R^{2} = \frac{\left[l\sum_{i=1}^{l} \hat{y}_{i} y_{i} - \sum_{i=1}^{l} \hat{y}_{i} \sum_{i=1}^{l} y_{i}\right]^{2}}{\left[l\sum_{i=1}^{l} \hat{y}_{i}^{2} - (\sum_{i=1}^{l} \hat{y}_{i})^{2}\right] \left[l\sum_{i=1}^{l} y_{i}^{2} - (\sum_{i=1}^{l} y_{i})^{2}\right]}$$
(9)

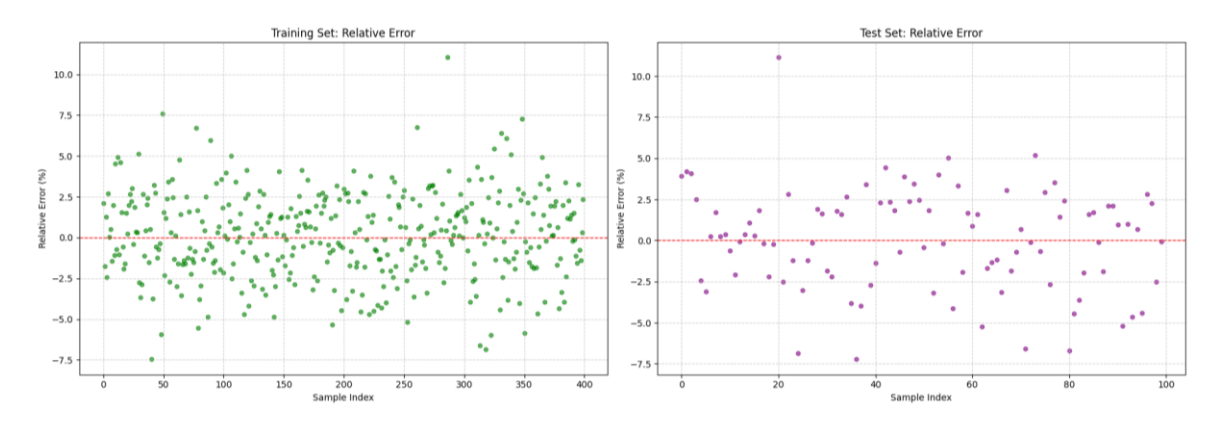
In the above formula, $\hat{y}_i(i=1,2,...,n)$ represents the predicted value of the *i*-th sample, while $y_i(i=1,2,...,n)$

denotes the corresponding true value. For the relative error E, smaller values indicate closer proximity to the true values and better model performance. The Mean Absolute Error (MAE) measures the average absolute deviation between predicted and true values as a nonnegative metric, where smaller MAE values correspond to superior models. The Root Mean Square Error (RMSE), a key regression metric, quantifies the magnitude of prediction errors, assigning higher weights to larger errors; like MAE, smaller values are preferable. The coefficient of determination (R^2) ranges within [0,1], with values closer to 1 indicating better model performance and vice versa.

Figure 9 presents the training and prediction results of the BPNN model. As shown in (a) and (b), the model successfully captures the primary fluctuation trends in both the training and test datasets. Notably, the predicted values on the test set demonstrate closer alignment with the true values compared to the training set. The reduced sample size of the test set results in less complex data fluctuations relative to the training set. Panels (c) and (d) display the model's relative errors, which predominantly fluctuate within $\pm 10\%$, indicating minimal errors for most samples. Remarkably, the test set's relative errors are further constrained within $\pm 5\%$, demonstrating the model's reliability and high predictive accuracy for crack density estimation.



a) the true and predicted values of the training set b) the true and predicted values of the test set



c) corresponding relative errors of the training set d) corresponding relative errors of the test set

Figure 9: Training and prediction results of BPNN for crack density

As evident from Figure 10, the residuals are predominantly concentrated within ± 0.01 , indicating the

model maintains excellent fitting capability with consistent stability.

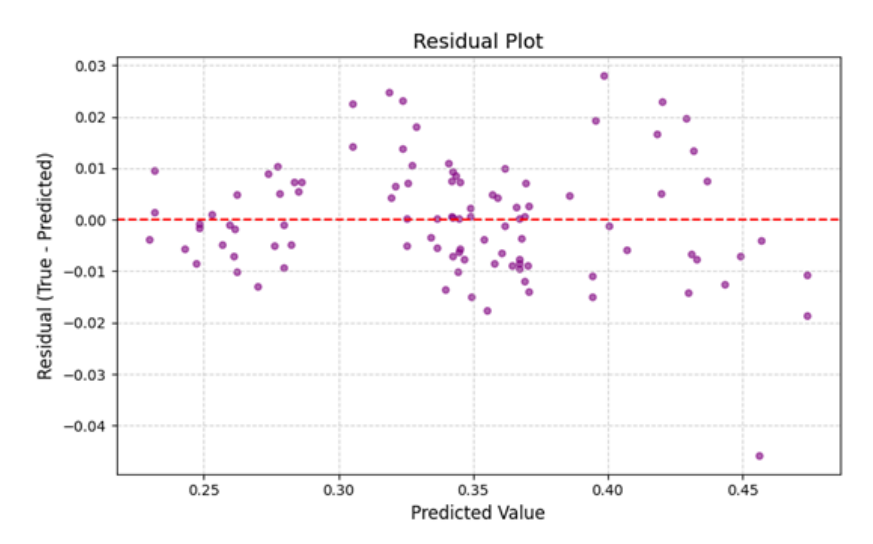


Figure 10: Residual plot of prediction samples

As shown in Table 9, the model's MAE, RMSE, and R^2 scores are presented. On the training set, the model achieves an R^2 of 0.9772, while on the test set, the R^2 is 0.9644, demonstrating strong fitting capability to the

training data and reliable prediction of crack density in Ni60 self-fluxing alloy powder laser cladding layers within an acceptable error margin. Furthermore, the training set shows MAE and RMSE values of 0.0071 and

0.0089, respectively, compared to 0.0085 (MAE) and 0.0111 (RMSE) for the test set. The minimal discrepancy between these metrics indicates robust predictive

performance in practical applications, with maintained effectiveness on random data samples.

Table 9: Performance metrics (R2, MAE, RMSE) for training and test sets

| | Coefficient of | mean absolute error | root mean |
|--------------|---------------------|---------------------|---------------------|
| | determination R^2 | (MAE) | square error (RMSE) |
| Training set | 0.9772 | 0.0071 | 0.0089 |
| Test set | 0.9644 | 0.0085 | 0.0111 |

3.5 Comparative analysis with alternative models

Based on the aforementioned analysis, we evaluated multiple machine learning algorithms-including KNN regression, Ridge regression, XGBoost regression, AdaBoost regression, CatBoost regression, Random Forest regression, LSTM regression, BiLSTM-AdaBoost regression, and CNN regression-on the same dataset and compared their performance with BPNN regression. The R², MAE, and RMSE values for each model are summarized in Table 10.

Table 10: Comparative results of crack density prediction on the test set

| Model name | R ² | MAE | RMSE |
|--------------------|----------------|---------|---------|
| KNN | 0.95002 | 0.00017 | 0.01301 |
| ridge regression | 0.88528 | 0.00039 | 0.01971 |
| XGboost regression | 0.92974 | 0.00024 | 0.01543 |
| ADA boost | 0.92604 | 0.00025 | 0.01583 |
| Catboost | 0.94618 | 0.00018 | 0.01543 |
| Random forest | 0.93593 | 0.00022 | 0.01472 |
| LSTM | 0.90605 | 0.01293 | 0.01784 |
| BiLSTM-AdaBoost | 0.91265 | 0.01313 | 0.01720 |
| CNN | 0.94571 | 0.00819 | 0.01356 |
| BP Neural Network | 0.96445 | 0.01109 | 0.00853 |

4 Discussion

The relationship between process parameters and crack susceptibility in laser cladding involves complex nonlinear interactions. The Backpropagation Neural Network (BPNN) was selected for this study to model the mapping between three key process parameters (powder feed rate, overlap ratio, and scanning speed) and crack density, owing to its exceptional nonlinear fitting capability and adaptive feature learning through error backpropagation that continuously optimizes network weights and thresholds to achieve high-precision modeling. Given the high cost and time-consuming nature of laser cladding experiments, orthogonal experimental designs are typically employed to investigate parameter-crack density relationships. However, neural networks like BPNN require substantial training samples for effective learning, which was addressed in this study through Kernel Density Estimation (KDE)-based data augmentation.

Experimental results (Tables 9-10) demonstrate that the BPNN prediction model achieves test set errors within ±5%, with MAE and RMSE values of 0.85% and 1.11% respectively. Comparative analysis with KNN regression, ridge regression, XGBoost regression, AdaBoost regression, CatBoost regression, random forest regression, LSTM regression, BiLSTM-AdaBoost regression, and CNN regression confirms BPNN's superior performance, evidenced by its highest R² score of 0.96445. This superiority stems from BPNN's three-layer architecture employing nonlinear activation functions (ReLU/Swish) that effectively approximate the complex multi-parameter interactions in laser cladding crack prediction scenarios.

The proposed method effectively addresses the critical challenges of process parameter optimization and crack density prediction in laser cladding, demonstrating significant value for fabricating high-quality nickel-based cladding layers. Furthermore, this research offers valuable insights for cladding processes involving similar materials (titanium alloys or other superalloys). By

establishing a BPNN-based mapping between process parameters and target performance characteristics, the study provides a universal research paradigm for precise "process-performance" regulation additive manufacturing, particularly enhancing process development efficiency for high-cost, high-precision manufacturing scenarios. Although this study has achieved significant results, there are still some potential limitations. The proposed method in this research lacks sufficient real-time optimization capability and an online learning mechanism, which hinders the model's selfadaptive iterative optimization ability in practical production environments. In future research, it will be essential to investigate elastic network structures with incremental learning capabilities and integrate online sequential learning algorithms to enhance the model's generalization ability and adaptability in engineering applications.

5 Conclusion

This study focuses on the laser cladding of Ni60 powder on 45# steel surfaces. By employing orthogonal experimental design combined with BP neural network modeling, we systematically investigated the nonlinear mapping relationship between process parameters (such as laser power, scanning speed, and powder feed rate) and crack density in the cladding layer. Through network training, learning, and predictive fitting, the reliability of the model was verified, providing a feasible solution for preparing crack-free nickel-based cladding layers. The results demonstrate that the BP neural network-based prediction model exhibits strong generalization performance on the test set, with a coefficient of determination (R2) of 0.9644, indicating excellent fitting capability. Additionally, the mean absolute error (MAE) and root mean square error (RMSE) were 0.0085 and 0.0111, respectively, confirming the model's predictive stability.

Through comparative analysis with various other regression algorithms-including KNN regression, ridge regression, XGBoost regression, AdaBoost regression, CatBoost regression, random forest regression, LSTM regression, BiLSTM-AdaBoost regression, and CNN regression-the BPNN (Backpropagation Neural Network) model demonstrated superior stability and accuracy. This finding validates the feasibility of integrating theoretical modeling with experimental validation, offering a promising new approach for preparing crack-free nickel-based cladding layers.

Further analysis indicates that conventional backpropagation (BP) neural networks exhibit limitations in processing high-dimensional parameter interactions, manifesting as slow convergence rates and susceptibility to local optima. Moreover, the model necessitates complete retraining when applied to new alloy powder systems. To enhance the predictive accuracy of the

network model, subsequent research could employ convolutional neural networks (CNNs) to extract morphological features from cladding layer images for improved parameter correlation modeling, while exploring Vision Transformer (ViT) architectures to integrate multimodal data, combining process parameters with molten pool dynamic monitoring images. Additionally, an online learning system could be implemented to enable dynamic closed-loop control of process parameters through real-time acquisition of spectral signals and thermal imaging data during the cladding process.

References

- [1] Li KQ, Li T, Ma M, Wang D, Deng WW, Lu HT. Laser cladding state recognition and crack defect diagnosis by acoustic emission signal and neural network. Optics & Laser Technology, 2021, 142(35):107161. https://doi.org/10.1016/j.optlastec.2021.107161
- [2] Zhao K, Liang XD, Wang W, Yang P, Hao YB, Zhu ZL. Multi-objective optimization of coaxial powder feeding laser cladding based on NSGA-II. Chinese Journal of Lasers, 2020, 47(1), 0102004. https://doi.org/10.3788/CJL202047.0102004
- [3] Wu J. Analysis of the main factors affecting the quality of laser cladding layer. Mechanical Manufacturing and Automation, 2004, (04): 52-56. https://doi.org/10.3969/j.issn.1671-5276.2004.04.018
- [4] Xu HY. Research on Solid Forming Control Process of 316L Stainless Steel Laser Cladding. Dalian University of Technology, 2018. DOI: CNKI: CDMD: 2.1018.869314
- [5] Xue S. Building material defect detection and diagnosis method based on big data and deep learning. Informatica, 2024. 48(16). https://doi.org/10.31449/inf.v48i16.6433
- [6] Yan SY. Crack sensitivity and evaluation method of Ni based alloy laser cladding layer. China University of Petroleum (East China), 2016.
- [7] Li GQ, Wang LF, Zhao L, Zhu GX, Shi SH. Research progress on crack problems in laser cladding layers. Hot Processing Technology, 2021, 50 (16): 13-17. https://doi.org/10.14158/j.cnki. 1001-3814.20192189
- [8] Ni LB, Liu JC, Wu YT, Yan C. Optimization of laser cladding process based on neural networks and particle swarm optimization. China Laser, 2011, 38 (02): 99-104. https://doi.org/10.3788/CJL201138.0203003
- [9] Huang AG, Li G, Wang YY, Li L, Li ZY. Prediction of characteristics and properties of aluminum alloy laser cladding layer based on artificial neural network. China Laser, 2008, (10): 1632-1636.

- https://doi.org/10.3321/j.issn:0258-7025.2008.10.039
- [10] Jiang SJ, Liu WJ, Nan LL. Prediction of laser cladding height based on neural networks. Journal of Mechanical Engineering, 2009, 45(03): 7. https://doi.org/10.3901/JME.2009.03.269
- [11] Yang DH, Ma L, Huang WD. Prediction of surface quality of laser stereoscopic forming parts based on artificial neural networks. China Laser, 2011, 38 88-93. https://doi.org/10.3788/CLJ201138.0803004.
- [12] Lei KY, Qin XP, Liu HM, Ran Y. Prediction of characteristic parameters of broadband laser cladding pool based on neural network. Optoelectronics and Laser, 2018, 29 (11): 1212https://doi.org/10.3901/10.16136/j.joel.2018.11.009
- [13] Liu GC, Huang B. Prediction of morphology of nickel based alloy cladding coating based on GA-BP neural network. Applied Laser, 2018, 38 (4): 9. DOI: CNKI: SUN: YJJG. 0.2018-04-004
- [14] Zhang L, Chen XM, Liu W. Formation mechanism and sensitivity of cracks in Ni based alloys by laser cladding. Advances in Laser and Optoelectronics, 2019, 56 (11): 176-183